Clays and Clay Minerals, Vol. 28, No. 1, 19–28, 1980.

INTERFACIAL WATER STRUCTURE IN MONTMORILLONITE FROM NEUTRON DIFFRACTION EXPERIMENTS

R. K. HAWKINS

Canada Centre for Remote Sensing, 2464 Sheffield Road
Ottawa, Ontario K1A 0E4, Canada

P. A. EGELSTAFF

Department of Physics, University of Guelph
Guelph, Ontario N1G 2W1, Canada

Abstract—Neutron diffraction measurements for a preferentially oriented aggregate slab sample of deuterated Na-montmorillonite from Upton, Wyoming, are described for a series of clay-water contents ranging from 0 to 500 mg/g. A neutron wavelength of 2.39 Å was used with extended detectors to collect much of the "out of plane" component of the diffraction peak intensities.

The diffraction pattern intensities from the 00ℓ planes of the clay, corresponding to a reflection geometry, are a strong function of sample water content and show a variation in basal spacing from 9.8 to 19.0 Å. The hk reflections from transmission geometry measurements show, however, that the lattice a and b axes are constant within experimental uncertainty (0.02 Å) over the range in water content and their intensities vary only by a few percent. In this geometry, a broad, water-like diffraction pattern was noted as a background under the usual hk peak intensity series. This underlying water-like pattern varies in proportion to the sample water content.

Data reduction steps included consideration of background removal, multiple scattering, flux normalization, and attenuation of scattering due to sample thickness. Analysis of the reduced data revealed that the clay-water has a "liquid-like" ordering, with a density increase of approximately 5% over bulk water. An association between a few interlayer water molecules and the silicate superstructure is indicated by the slight change in the hk band intensities, but this change seems to be complete at water contents below 100 mg/g. Fourier analysis of the basal peak series from the dry clay shows that the hydrogens of the lattice hydroxyl groups lie in the same basal plane as their associated oxygen atoms.

Key Words—Clay-water system, Hydroxyl orientation, Interlayer water, Montmorillonite, Neutron diffraction.

INTRODUCTION

It is well known (e.g., Grim, 1968) that water molecules penetrate between the silicate layers of expanding clay minerals forcing the unit cells to swell. The crystal binding forces across the interlayer region are very weak in a smectite, and the mineral may be considered to be two-dimensional, consisting of thin platelets of irregular shape.

The register between adjacent silicate layers is poor, but the structure is not completely turbostratic (Güven, 1975; MacEwan, 1961). There is, however, a repeated basal plane distance d, between parallel silicate units. The d-spacing of a dried montmorillonite is ~10 Å, and the mineral swells uniformly until it reaches a spacing of ~20 Å. At larger spacings, the swelling homogeneity decays, and a range of values can occur (Norrish, 1954). These physical properties make clay-water systems experimentally attractive for the study of interfacial water structure.

X-ray diffraction research of the structure of clay-water complexes has focused mainly on vermiculite since this mineral forms large single crystals and appears to swell in definite hydration steps. Mathieson and Walker (1954) found that water molecules form two planes above and below the interlayer cations and that they maintain octahedral coordination with these cations. Within the planes, the oxygen sites form hexagonal arrays. Telleria *et al.* (1977) made similar conclusions regarding the structure within the water plane but found for a less expanded vermiculite that a single plane of water exists at the center of the unit-cell interlayer with cations on either side.

Little discussion has been devoted to hydrogen locations either within the lattice itself or in connection with the interlayer water molecules in the X-ray diffraction work on clay even though many inferences have been made from infrared data (Farmer and Russell, 1971) and other techniques that hydrogen-bond linkages may exist in the interlayer region. This lack of structural information from X-ray diffraction measurements with respect to hydrogen is because hydrogen has only one electron and therefore offers the least X-ray scattering signal of all the elements. The scattering power of each atom is changed when neutrons are used so that hydrogen scattering is a major component of the neutron scattering intensity in contrast to the X-ray situation. Isotopic substitution provides an additional means of changing the atomic scattering power

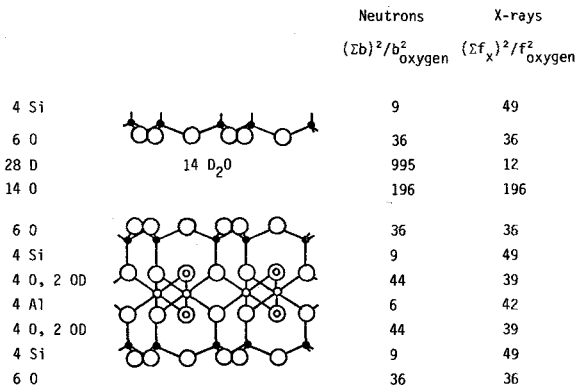

Figure 1. Scattering power of layers of atoms in the clay structure. For X-rays a neutral atom model has been used, since the extent of the covalent charge transfer is uncertain.

since the neutron is scattered by the nucleus of the atom. Neutron diffraction can therefore provide new structural information about the clay-water system and is especially suited to a study of intercalated water. Figure 1 shows the composition and relative scattering power of planes of atoms for X-rays and neutrons in an idealized montmorillonite lattice swollen with heavy water. Heavy water is used because deuterium has a larger coherent scattering cross section (responsible for diffraction effects) than hydrogen with neutrons, and because the background due to incoherent scattering is smaller. The swelling of 20 Å in this illustration corresponds to ~14 water molecules per pseudo unit cell. The crystal is shown as a projection on to the *bc* plane. In listing the X-ray scattering power, neutral atoms have been assumed at all sites; this is an oversimplification, and there is some uncertainty over the interpretation of X-ray intensities. No such ambiguity arises with neutron intensities since these are independent of the electron distribution. Figure 1 demonstrates that neutrons are very much more sensitive to interlayer water (especially the deuterium) and that water scattering itself is more evenly divided between the deuterium and oxygen.

An initial study of clays by Cebula *et al.* (1979) indicated that neutron diffraction is indeed practical, even though typical neutron fluxes are much less intense than conventional X-ray sources. Inelastic neutron scattering (Hunter *et al.*, 1971; Olejnik and White, 1972) proved useful in elucidating some dynamical properties of the absorbed water molecules. The present work was undertaken to study the structure of the interlayer water absorbed in Na-montmorillonite using the neutron diffraction technique.

EXPERIMENTAL

Sample preparation

Montmorillonite from Upton, Wyoming (J. C. Lane tract), was chosen for study on the basis of its wide use in associated research and its ready availability. Ross and Mortland (1966) reported the following formula for this material:

$$Na_{0.64}[Al_{3.06}Fe_{0.32}Mg_{0.66}](Al_{0.1}Si_{7.9})O_{20}(OH)_4.$$

The raw mineral was purified and treated according to the method of Posner and Quirk (1964). Chemical analysis showed no fixed potassium in the sample demonstrating that the raw bentonite contained no interstratified mica. The <2-μm fraction was removed by sedimentation. This fraction was saturated with NH_4^+, freeze-dried, and deuterated by heating the freeze-dried, NH_4-clay to 350°C in the presence of heavy water vapor at 17 torr (Russell *et al.*, 1970). The clay was transferred to a 1 N non-aqueous solution of NaI-acetone and washed to resaturate the mineral with Na-cations. Acetone aids both in the reswelling of the clay after the heat treatment (Brindley and Ertem, 1971) and in preventing a rehydrogenation of the lattice through exposure to free hydrogen while the clay remains in the acid ND_4-form. Infrared analysis for the lattice-OH, and lattice-OD absorption peaks near 3640 and 2690 cm^{-1} showed that even at room temperature the acid form of the clay exchanged lattice hydrogen for deuterium while the Na-saturated clay remained stable against this isotopic exchange. This property suggested both the acetone-exchange medium and the use of the Na-saturated clay.

Following its resaturation with Na in the NaI–acetone solution, the clay was washed free of excess Na in distilled (light) water using dialysis tubing, and a sample was prepared by slowly drying 500 ml of a 1% (by weight) suspension in a teflon-lined container. Warm air was circulated over the evaporating surface, but at no time was the suspension temperature allowed to rise above 37°C. Approximately two weeks drying time was required. The slow evaporation rate was necessary to produce macroscopically uniform specimens with a high degree of preferred orientation. The neutron specimen was composed of a stack of several clay sheets (total dry mass =

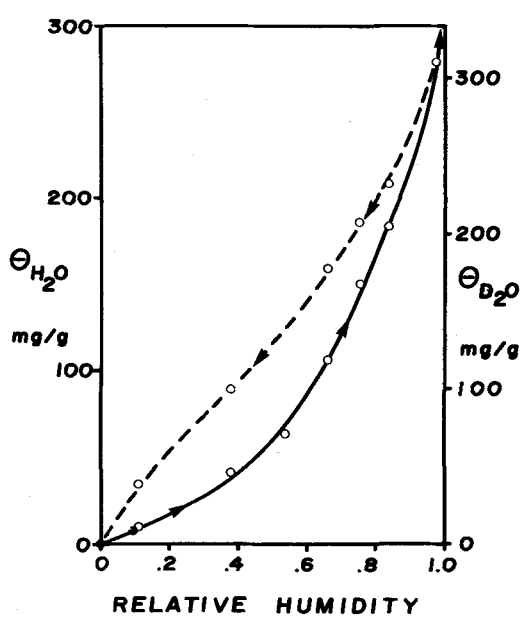

Figure 2. Hydration curves for deuterated Na-montmorillonite. θ_{D_2O} and θ_{H_2O} are the sample water contents of heavy and light water respectively, expressed as a fraction of the dry weight of the deuterated clay.

https://doi.org/10.1346/CCMN.1980.0280103 Published online by Cambridge University Press

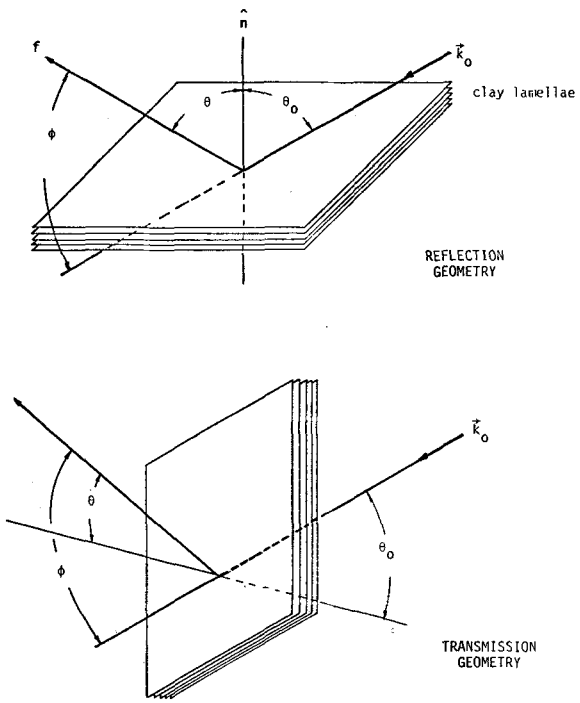

Figure 3. Experimental sample geometries. The wave vectors for the incident and scattered beams are $\vec{k}_0$ and $\vec{k}_f$ respectively, with the scattering vector $\vec{Q} = \vec{k}_f - \vec{k}_0$. Vector $\hat{n}$ is normal to the clay lamellae. In the reflection geometry, the neutron momentum transfer, $h'\vec{Q}$, is perpendicular to the lamellae while it is parallel to them in the transmission geometry.

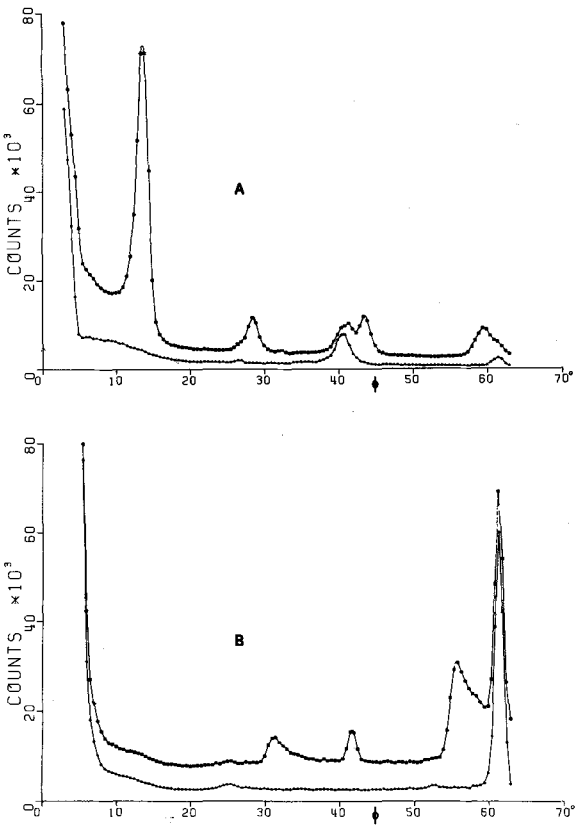

Figure 4. Raw diffraction data from dry deuterated clay in reflection (A) and transmission geometries (B). In each of the two sets of data, the lower curve represents the container background while the upper curve is for the container and clay sample together.

5.68 g) which were dried from suspension and held in a thin (0.8 mm) aluminum vessel, sealed to the atmosphere.

To follow the change of the neutron diffraction pattern as a function of the water content, the sample was allowed to reach equilibrium with the vapor above a saturated solution in a desiccator. The water content was regulated by changing the kind of salt solution. Equilibrium was reached in this chamber in two days, although longer periods were required for samples with high water contents. The sample was then weighed quickly and sealed into the sample vessel for the diffraction measurement. Very high water contents were achieved by first equilibrating samples in a 98% relative humidity (RH) environment and then transferring them to a 100% RH chamber. Water content was monitored by weighing the samples until the desired amount was reached. Dry samples were produced by first evacuating them to 10^{-4} torr and then heating them to 110°C, maintaining this vacuum.

Water-vapor absorption characteristics for the deuterated clay sample are shown in Figure 2. A hysteresis can be seen in the wetting and drying cycle. The best indicator of the water state of the sample is therefore the gravimetric water content, θ_w, and not the equilibration RH.

Neutron diffraction measurements

Neutron diffraction and transmission data were taken using the University of Guelph neutron diffractometer located at the D-3 port of the NRU reactor at the Chalk River Nuclear Laboratories at Chalk River, Ontario. Simultaneous measurement of 5 scattering angles spaced at ~1° intervals was made using counters of 40 cm length which rotated about the sample to cover a total angular range of ~120°. The neutron wavelength selected was 2.386 Å. Satisfactory counting statistics and convenient run-durations were obtained by counting for 5 min at each setting, stepping the spectrometer in 0.5° increments.

For the reflection geometry illustrated in Figure 3, a beam width of 3 mm was used. A beam width of 25 mm was used for the transmission geometry. In each geometry, the sample was rotated in the beam to maintain a constant orientation with respect to the neutron momentum transfer, $h'Q$, as the spectrometer rotated. (In this expression, h' is the Planck constant divided by 2π.)

Rocking curves of samples were taken in the reflection geometry to establish the degree of preferential ordering in the aggregate. The full width at half maximum of these curves was ~18°. This wide effective mosaic allowed simultaneous measurement of several scattering angles and also justified the use of long detectors to receive the scattering for the partially oriented samples which consist of diffraction arcs, segments of the normal powder cones. This aspect of the scattering had important implications in the data analysis, particularly for the Lorentz factor which is discussed more fully below.

Diffraction patterns were taken of an empty sample container, so that background scattering could be removed; of a vanadium standard; and of heavy water. Most of the clay-water diffraction measurements were made with deuterated clay swelled with heavy water, but additional data were taken with deuterated clay containing light water at 66% RH and

https://doi.org/10.1346/CCMN.1980.0280103 Published online by Cambridge University Press

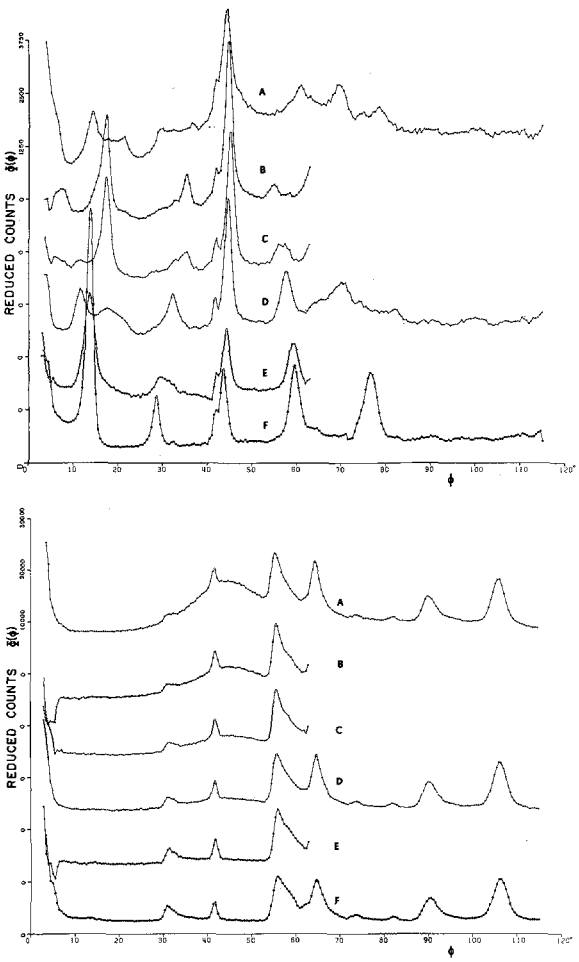

Figure 5. The reduced intensity function $\Phi(\phi)$ defined in Eq. (1), at 6 different water contents for (upper set of curves) deuterated clay in the reflection geometry and (lower set of curves) deuterated clay in the transmission geometry. (A = 100% RH, B = 98% RH, C = 75% RH, D = 66% RH, E = 38% RH, F = dried clay.)

hydrogenous clay containing heavy water at 0 and 75% RH. In all cases, samples with slab geometry were used. The heavy water was supplied by Stohler Isotopes, Montreal, and tested at 99.5% deuterium.

Raw diffraction patterns and their backgrounds from ϕ = 0° to 70° are indicated in Figure 4 for dried clay. The sharp rise at small angles is due to scattering of the beam by the counter shield. The expected contrast between the two experimental geometries and the lack of random orientation component demonstrate a high degree of preferred orientation in the sample. The heavy water yielded a typical diffraction pattern with a broad first order diffraction peak. (See Page and Powles, 1971.)

Data were taken for six conditions between dry and 100% RH and are shown in a reduced form after subtraction of background in Figure 5. The change in the diffraction patterns of the raw clay as water entered the clay differs for the two experimental geometries. For the reflection geometry, the diffraction peaks change both in position and in intensity and appear unrelated to the pattern of either the dried clay or pure water. The diffraction pattern for the transmission geometry, however, resembles a combination of the patterns of dried clay and the heavy water.

DATA REDUCTION AND ANALYSIS

Neutrons which arrive at the detectors can be from several sources: stray background from within the reactor hall; scattering from air along the incident-beam flight path; scattering from the container; or scattering from the sample itself. They may also be singly or multiply scattered. The finite thickness of the sample causes multiple scattering and is also responsible for an attenuation of both the undeviated and scattered neutrons. Only the once-scattered radiation from the sample alone, where self-attenuation is negligibly small, is of interest.

Reduced data were calculated from the raw measurements according to the formula:

$$\Phi(\phi) = I_0 N \frac{d\sigma}{d\Omega} = \frac{I_{s+c}(\phi) - I_c(\phi) A_{c,s}}{A_{s,c} A_{s,s} \sec \theta_0 c(\phi)} \qquad (1)$$

Here ϕ is the scattering angle; I_0 is the total incident neutron flux; N is the number of scattering units in the beam, each with a differential cross section of $d\sigma/d\Omega$; $I_{s+c}(\phi)$ and $I_c(\phi)$ are the raw scattering seen by the sample with its container and the container alone. The A_{sc} are appropriate slab absorption factors using the notation of Paalman and Pings (1962). The sec θ_0 factor is a correction for the effective sample volume in the beam as the incidence angle, θ_0, defined in Figure 3, is altered by half angling during the scan. The angular calibration factor, $c(\phi)$, is derived by comparing theoretical and measured values for the standard vanadium, and for the instrument used, is independent of ϕ. When the corrections inherent in Eq. (1) are applied to the raw data, the curves shown in Figure 5 emerge.

Removal of container background peaks and the relative change in the size of the first diffraction peak for the reflection geometry, are effects easily seen for the dried clay by comparing the curves in Figure 4 and those in the upper part of Figure 5. The relative peak intensities in the transmission data (Figure 5, lower set of curves) however, remain largely unchanged. Because of this systematic difference in the data, the analysis is divided into two sections corresponding to the different experimental geometries.

Reflection geometry analysis

The interpretation and analysis of the reflection data are based on the one-dimension Fourier analysis of the $\Phi_{00\ell}(\phi)$ series of diffraction peaks. This series is clearly visible in the diffraction pattern of the dry clay with the peak assignments being less obvious at higher clay-water contents. The 00ℓ peaks should occur at ϕ angles

https://doi.org/10.1346/CCMN.1980.0280103 Published online by Cambridge University Press

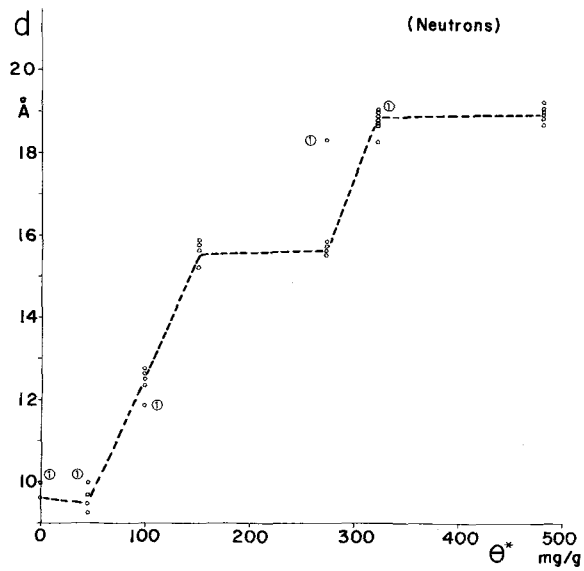

Figure 6. Spacings calculated from Eq. (2), using the (00ℓ) peak positions of the neutron diffraction data. The dashed line has been drawn through the weighted mean of the peaks for $\ell > 1$, and the first order data are indicated by the symbol ①.

corresponding to the basal spacing, d, given by the Bragg relation.

$$d = \lambda\ell/2 \sin(\phi_0/2) \quad (2)$$

Here λ is the neutron wavelength and ϕ_0 is the scattering angle of the peak center. Application of this formula led to Figure 6.

The dispersion of the plotted points cannot be attributed entirely to uncertainty of peak measurement nor of peak assignments but probably represents real inhomogeneity in the sample spacings due to interstratification. The d-value variation with the order of diffraction, ℓ, in the neutron data is much less than from X-ray diffraction analysis carried out on the same sample or as indicated by other X-ray investigations (Margheim, 1977).

The 00ℓ peak intensities are given by the expression:

$$\Phi_{00\ell} \propto T^2(\phi)\, L(\phi)\, F^*_{00\ell}(Q)\, F_{00\ell}(Q) \quad (3)$$

where $T(\phi)$ is the temperature or Debye-Waller factor of the lattice, $L(\phi)$ is the Lorentz factor, and $F_{00\ell}(Q)$ is the unit cell structure factor. The temperature and structure factors have well known expressions (e.g., Azaroff, 1968), and usually the Lorentz factor is a simple trigonometric function. For the preferentially oriented aggregate sample, this factor is complicated and requires special consideration as demonstrated by Reynolds (1976). For the conditions of our sample and spectrometer, a lengthy analysis revealed (Hawkins, 1978) that the expression:

$$L(\phi) = \csc\phi \operatorname{erf}[K\alpha_{max}\cos(\phi/2)] \quad (4)$$

adequately describes the correction. This expression is a simplification of Eq. (5) of Reynolds (1976). In this equation,

$$\alpha_{max} = \cos^{-1}[1 - (w/2R \sin\phi)] \quad \text{or} \quad \sin^{-1}(L/2R \sin\phi)$$

whichever is smaller. L and w are the detector dimensions, R is the diffractometer radius, and K describes the distribution of crystallite orientations within the aggregate. $F_N(\epsilon)\, d\Omega$ is the probability of finding a platey crystallite in the sample whose normal lies inclined to the slab normal at an angle ϵ, in the solid angle range $d\Omega$. The expression is assumed to be gaussian with $F_N(\epsilon) = A \exp(-K^2\epsilon^2)$. Eq. (4) represents a major correction to the measured peak intensities for the basal plane reflections. At $\phi = 10°$, $L(\phi)$ introduces a factor of 10 into the intensity calculation compared to 1 at 90°; but this range is less than the corresponding values for the usual X-ray case. This distortion is also responsible for a skewness in the measured diffraction pattern which is especially apparent at low scattering angles. It shifts the real peak center toward the origin at low scattering angles, and a correction is necessary. Such a correction was made to the spacing data in Figure 6.

Once the Lorentz and temperature factors have been estimated, the modulus of the structure factor may be determined within a constant factor. Because the clay is centrosymmetric across the basal planes, $F_{00\ell}(Q)$ values are real, and the phase factor $s(\ell) = \pm 1$. (The choice of sign was determined through model comparisons.) Hence,

$$F_{00\ell}(Q) = s(\ell) F_{00\ell} \quad (5)$$

where $F_{00\ell} = \{\Phi_{00\ell}/[L(\phi)T^2(\phi)]\}^{1/2}$

The neutron-relative-scattering-density profile, $\rho_s(z)$, across basal planes may now be constructed from the structure factor data by the relation,

$$\rho_s(z) \propto \frac{2}{d} \sum_{\ell} s(\ell) F_{00\ell} \cos\left\{\frac{2\pi\ell z}{d}\right\} \quad (6)$$

Figure 7 is a neutron-scattering-density profile for the unit cell of the hydrogenous and deuterated clay in a dry and wet state; the resolution is ~1 Å. These curves should be contrasted with the X-ray diffraction results of Pézérat and Méring (1967). The atomic structure of the silicate is better resolved in X-ray diffraction profiles because the sheets of atoms have closer X-ray scattering powers (as was anticipated in Figure 1). The neutron profiles for the deuterated and hydrogenous clay indicate that the hydrogen atoms in the lattice hydroxyl groups lie very nearly in the same z-plane as

https://doi.org/10.1346/CCMN.1980.0280103 Published online by Cambridge University Press

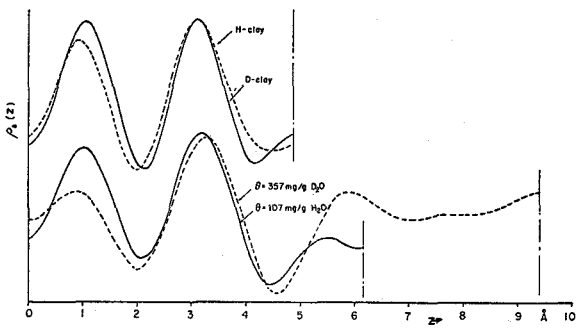

Figure 7. Scattering density profiles from neutron diffraction data, with a resolution of ~1 Å. The (dry clay) profiles are from hydrogenous (H-clay) and deuterated clay (D-clay). The vertical center lines indicate the unit-cell symmetry axis. The curves have been normalized to equate the maximum amplitude of each profile.

their associated oxygens. The interlayer region in Figure 7 shows a striking similarity with the results of Pézérat and Méring (1967). The relative lack of structure of $\rho_s(z)$ in the region indicates that the interlayer is *not* highly ordered into definite planes of atoms as has been anticipated by those who have postulated layering from the hydration studies.

The transform of Eq. (6) can be used to predict the measured 00ℓ diffraction peak intensities by modelling the atomic structure across the clay layers. This technique was used to determine the lattice hydrogen locations in the dry clay. Z coordinates determined by other X-ray diffraction investigations (Mathieson and Walker, 1954; Pézérat and Méring, 1967; Cradwick, 1975) for all non-hydrogen atoms were first used to optimize the X-ray diffraction results from the deuterated clay since these are largely independent of the hydrogen present in the sample. Then the hydrogen positions alone were varied to allow the best agreement for the neutron measurements for the same series of diffraction peaks. For the deuterated clay, optimum positions were in the same plane as the associated oxygens within ±0.01 Å. Table 1 shows the agreement reached and Table 2 gives the *c*-axis coordinates chosen for the dry

Table 1. Intensity ratios of dry clay and model predictions.

Order (ℓ)	($\Phi_{00\ell}/\Phi_{001}$) model	($\Phi_{00\ell}/\Phi_{001}$) measured
1	1.000	1.000
2	0.173	0.21 ± .02
3	0.297	0.37 ± .03
4	0.596	0.53 ± .05
5	0.603	0.53 ± .04
6	0.027	0.022 ± .002

A complete tabulation of measured peak intensities is given by Hawkins (1978).

Table 2. Atomic coordinates of dry clay.

Layer species	z (Å)
$[Al_{3.06}Fe_{0.32}Mg_{0.66}]$	0.0
$O_4(OD)_2$	1.09
Si_4	2.70
O_6	3.27
$Na_{0.32}$	4.15

clay. In these calculations an isotropic temperature factor was used with B = 2.0 Å ($T(\phi) = \exp(-B/\lambda^2\sin^2\phi/2)$) for all atoms. B was chosen from results given by various authors (e.g., Mathieson, 1958; Telleria *et al.*, 1977) for vermiculite. No modelling was attempted for the wet samples because their diffraction pattern was no longer a discrete set of peaks.

Transmission geometry analysis

The broad liquid-like underlying pattern and the asymmetric diffraction peaks are distinctive features of the transmission geometry results. The diffraction peaks are designated by only two indices since the ideal two-dimensional crystal has no crystallographic *c*-axis. The form of the diffraction peaks as first explained by von Laue will be asymmetric and may be represented by the equation: (see also Kjems *et al.*, 1976).

$$\sigma_{coh}(\phi) = \frac{m_{hk}F^*_{hk}(Q)F_{hk}(Q)F_N(\epsilon)}{\sin(\phi/2)[\sin^2(\phi/2) - \sin^2(\phi_{hk}/2)]^{1/2}} \quad (7)$$

Here m_{hk} is the multiplicity factor for the reflection, $F_N(\epsilon)$ is an orientation related factor, and ϕ_{hk} is the scattering angle for the reflection. Eq. (7) can be seen to produce "saw-tooth" diffraction peaks, but applies strictly to an ideal (turbostratic) two-dimensional crystal only. For montmorillonite which has a limited degree of ordering between layers, no theory has been developed. Nevertheless, the inclusion of water in the interlayer which remains correlated in positions with the other atoms of the pseudo unit cell, must contribute to the structure factor in Eq. (7) and so change the measured hk peak intensities (*vide infra*).

Figure 8 is a recombination of the reduced data from the transmission geometry experiment. The lower curve from the dried clay is combined with the second curve from pure heavy water to produce a simulation of the measurement of the swollen clay. The heavy water curve is scaled to the equivalent thickness of heavy water content of the clay sample before it is added to the dry clay curve. (Because each curve has been corrected for sample self-attenuation, no absorption factor is required in the recombination.) The re-

https://doi.org/10.1346/CCMN.1980.0280103 Published online by Cambridge University Press

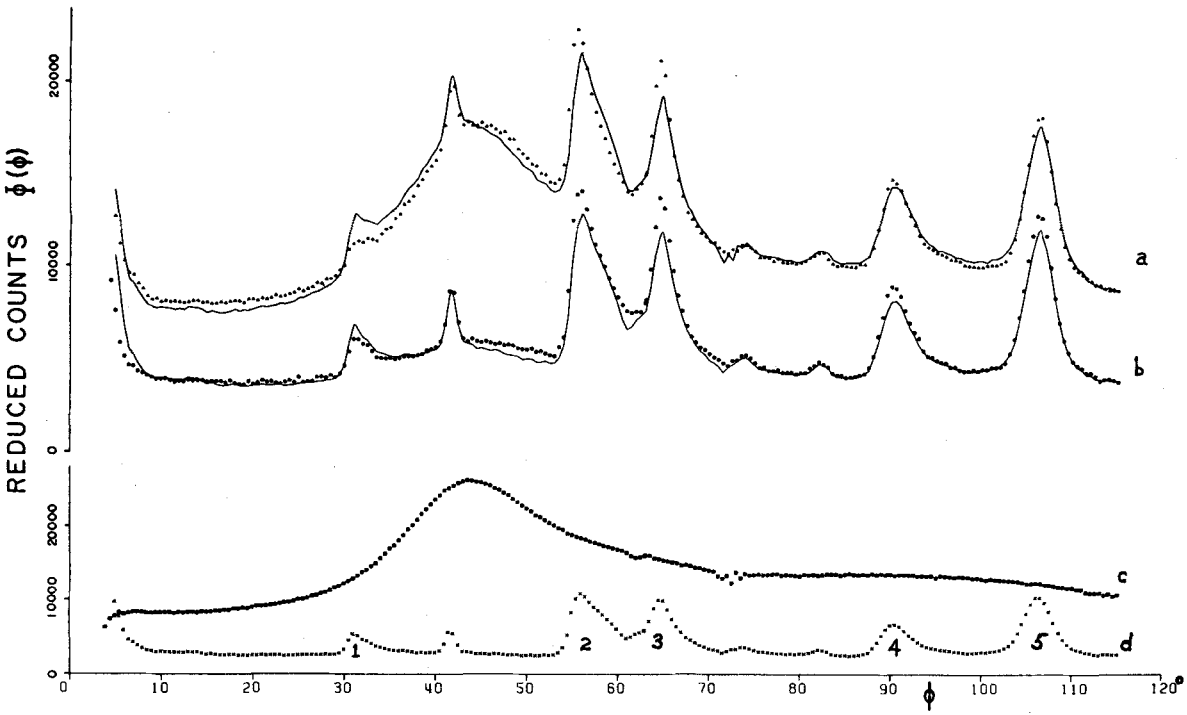

Figure 8. Comparison of the measured clay-water diffraction pattern and a mixture simulation of dry clay and water. Curve d is for dry clay and the numbered peaks may be indexed as follows: 1 = [11;02], 2 = [13;20], 3 = [22;04], 4 = [31;15;24], 5 = [06]. Curve c is for pure heavy water; curve b is for clay plus 107 mg/g of D_2O; and curve a is for clay plus 533 mg/g of D_2O. The full lines in the latter two cases are obtained by combining curves c and d in the given proportions.

combination results are the full lines to be compared with the experimental points.

The overall agreement is fairly good, but there are important discrepancies. First, it can be seen that no linear combination of the curves of the dry clay and the pure water is sufficient to reconstruct the pattern of the wet clay in detail. The measured clay-water peak also shifts to higher ϕ from its positions in the pure water case. Assuming the average spacing in the medium varies to be $\rho^{-1/3}$, where ρ is the liquid number density, this shift would represent a water density increase of ~5%. It is seen that the diffraction peaks are affected in different ways with the inclusion of the water. (Peak assignments marked on the pattern of the dry clay are from MacEwan (1961).) The 11;02 band appears to have decreased in intensity while the 06 peak increased. Finally, the hk peak positions are largely unaffected by the clay-water content. The 06 peak centroid position, in particular, remained constant to an experimental uncertainty of about ±.02 Å throughout the experiment and is consistent in this respect to measurements with X-rays (Margheim, 1977).

DISCUSSION

Profiles of the one-dimensional scattering densities in the interlayer region are relatively flat, and the transmission geometry diffraction pattern may be substantially reproduced by the superposition of the separated patterns of the water and the dry clay. Each of the results indicates that the interlayer region is not highly structured. There are, however, some outstanding features of the observed data that cannot be explained by the statement that the interlayer water is simply in a bulk state.

The intensities of the hk peaks from the transmission geometry, especially the 11 and 02, do change slightly as water enters the clay. This change may be explained only by a variation of the structure factor F_{hk} in Eq. (7), since the other quantities in the intensity relation remain fixed as can be seen by an examination of Eq. (8).

$$F_{hk} = \sum_j f_j e^K \qquad (8)$$

where $K = -i[2(hx'_j + ky'_j) + Q_\perp z_j]$,

x'_j, y'_j are the reduced coordinates of the atoms, z_j is the real coordinate, $Q_\perp$ is the component of the momentum transfer perpendicular to the clay layer on scattering, and f_j is the scattering length of the jth atom. The summation extends over all atoms in the pseudo-

https://doi.org/10.1346/CCMN.1980.0280103 Published online by Cambridge University Press

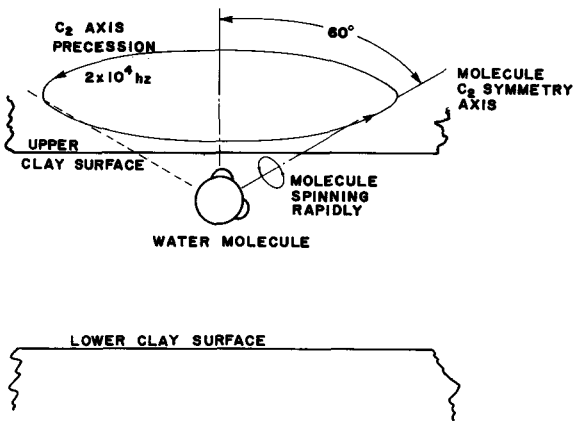

Figure 9. A model of spinning water molecules proposed by Fripiat and Stone (1978), on the basis of NMR data.

unit cell, and the average extends over all such cells. The associated Lorentz factor may change if the degree of preferential ordering in the sample is altered during swelling. Because the rocking curves for the sample in the dried or wetted states were essentially the same, no change in ordering is inferred.

If the interlayer material remains randomly distributed with respect to the silicate lattice atoms, its contribution to Eq. (8) is zero. For the transmission geometry $\langle Q_\perp \rangle = 0$, so that as long as the silicate itself remains unaltered in the *ab* plane, no change is expected in the hk peaks by the swelling of the clay under the assumption of bulk water filling. The exchangeable cations are believed to be released into the interlayer region when the clay expands. Their contribution to the peak intensity is small, however, and therefore cannot account for the observed changes. The explanation of the change in the hk peak intensities must therefore be that at least some of the atoms in the interlayer water molecules are spatially correlated with the silicate layers above and below. There cannot, however, be a complete epitaxy, both because the hk peak intensities are not changed appreciably and because the bulk water pattern persists. Close inspection of the series of reduced transmission diffraction patterns in Figure 5, reveals that any change that occurs in the two-dimensional diffraction peaks is complete at relatively low water contents. Presumably only a few of the initially absorbed water molecules are locked into an association with the lattice.

The presence of a solid-state water lattice in the interlayer, with different spacing than that of the silicate substructure, is also ruled out since this would lead to a new set of two-dimensional diffraction peaks in addition to those present from the lattice of the dry clay. Such behavior has been observed when gases are absorbed on grafoil in low temperature studies (Kjems *et al.*, 1976).

Fripiat and Stone (1978) suggested from NMR studies that interlayer water molecules associated with the clay lattice spin freely about an axis of fixed orientation which precesses as illustrated in Figure 9. The oriented molecules must have reduced translational freedom to those in bulk water since their diffusion constant which is approximately one-tenth of the bulk value (Hunter *et al.*, 1971; Olejnik and White, 1972). This model qualitatively accounts for most of the observed neutron diffraction results, since the spinning water molecules in the interlayer smooth out the density profile removing the correlation of the hydrogen (deuterium) positions with the lattice and packing constraints dictate the usual water-water correlations seen in the bulk-water pattern superposed on the lattice peaks. A similar explanation has been proposed for an analogous three-dimensional lattice situation in CBr_4 by Dolling *et al.* (1979). There, the carbon nuclei are fixed to lattice sites while the bromines are rotating. The resulting diffraction pattern has both lattice diffraction peaks and a liquid-like pattern from the bromine. More work is needed to verify this explanation quantitatively.

This study has produced new data concerning the water absorbed on the clay surfaces. The results argue against a highly structured interlayer water in rigid association with the silicate surfaces. Instead, the high selectivity of the neutrons has been used to show that the clay-water in Na-montmorillonite has a liquid-like structure and that it is only partially associated with the silicate.

Part of the analysis used here is based on determining intensities of Bragg reflections with standard formulae for crystal structure. It is evident, however, that the experimental data of Figure 5 do not support this view fully, and might be represented as a continuous curve rather than a set of discrete peaks. The interpretation of such a curve is involved and must treated elsewhere.

ACKNOWLEDGMENTS

The authors are grateful to Drs. B. D. Kay and M. B. McBride for advice in the sample preparation; to Messrs. G. H. Willis, J. F. Spicer, and T. J. Riddolls for construction of the neutron equipment; and to the staff of Atomic Energy of Canada Limited at Chalk River, Ontario, for assistance in the work at the NRU reactor. A discussion with Dr. L. Pascell of Brookhaven National Laboratory, was most helpful. The authors are indebted to Dr. L. Evans, Department of Land Resource Science, University of Guelph, for chemical analyses of the purified montmorillonite. R. K. Hawkins gratefully acknowledges the scholarship support of the Government of Canada and the Province of Ontario.

REFERENCES

Azaroff, L. V. (1968) *Elements of X-ray Crystallography:* McGraw-Hill, New York, 610 pp.

Brindley, G. W. and G. Ertem (1971) Preparation and solvation properties of some variable charge montmorillonites: *Clays & Clay Minerals* **19,** 399–404.

Cebula, D. J., Thomas, K. K., Middleton, S., Ottewill, T. H., and White, J. W. (1979) Neutron diffraction from clay-water systems: *Clays & Clay Minerals* **27,** 39–52.

Cradwick, P. D. (1975) On the calculation of one-dimensional X-ray scattering from interstratified material: *Clay Miner.* **10,** 347–356.

Dolling, G., Powell, B. M., and Sear, V. F. (1979) Neutron diffraction study of the plastic phases of polycrystalline SF_6 and CBr_4: *Molec. Phys.* **37,** 1859–1883.

Farmer, V. C. and Russell, J. D. (1971). Interlayer complexes in layer silicates: The structure of water in lamellar ionic solutions: *Trans. Farad. Soc.* **67,** 2737–2749.

Fripiat, J. J. and Stone, W. E. E. (1978) Water on the surfaces of clay minerals: Orientation, diffusion and proton exchange: *Phys. Chem. Liq.* **B7,** 349–373.

Grim, R. E. (1968) *Clay Mineralogy:* 2nd ed., McGraw-Hill, New York, 596 pp.

Güven, N. (1975) Electron-optical investigations on montmorillonites. I. Cheto, Camp Berteaux, and Wyoming montmorillonite: *Clays & Clay Minerals* **22,** 155–165.

Hawkins, R. K. (1978) A neutron diffraction study of clay-water structure: Ph.D. Thesis, University of Guelph, Guelph, Ontario, 295 pp.

Hunter, R. J., Stirling, G. C., and White, J. W. (1971) Water dynamics in clays by neutron spectroscopy: *Nature* **230,** 192–194.

Kjems, J. K., Passell, L., Taub, H., Dash, J. G., and Novaco, A. D. (1976) Neutron scattering study of nitrogen adsorbed on basal plane oriented graphite: *Phys. Rev.* **B13,** 1446–1462.

MacEwan, D. M. C. (1961) Montmorillonite Minerals: in *The X-ray Identification and Crystal Structures of Clay Minerals:* G. Brown, ed., Mineralogical Society, London, 143–207.

Margheim, J. F. (1977) Interrelations of b-dimension, water content and rheology of Na-smectites: Ph.D. Thesis, Purdue University, 87 pp.

Mathieson, A. M. (1958) Mg-vermiculite: A refinement and reexamination of the crystal structure of the 14.36 Å phase: *Amer. Mineral.* **43,** 216–227.

Mathieson, A. M. and Walker, G. F. (1954) Structure of Mg-vermiculite: *Amer. Mineral.* **39,** 231–255.

Norrish, K. (1954) The swelling of montmorillonite: *Disc. Faraday Soc.* **18,** 126–134.

Olejnik, S. and White, J. W. (1972) Thin layers of water in vermiculites and montmorillonites—Modification of water diffusion: *Nature* **236,** 15–16.

Paalman, H. H. and Pings, C. J. (1962) Numerical evluation of X-ray absorption factors for cylindrical samples and annular sample cells: *J. Appl. Phys.* **33,** 2635–2639.

Page, D. I. and Powles, J. G. (1971) The correlation of molecular orientation in liquid water by neutron and X-ray scattering: *Mol. Phys.* **21,** 901–926.

Pézérat, H. and Méring, J. (1967) Recherches sur la position des cations échangeables et de l'eau dans les montmorillonites: *C. R. Acad. Sci. (Paris)* **265,** 529–532.

Posner, A. M. and Quirk, J. P. (1964) The adsorption of water from concentrated electrolyte solutions by montmorillonite and illite: *Proc. Roy. Soc. (London)* **278A,** 35–56.

Reynolds, R. C. (1976) The Lorentz factor for basal reflections from micaceous minerals in oriented powder aggregates: *Amer. Mineral.* **61,** 484–491.

Ross, G. J. and Mortland, M. M. (1966) A soil beidellite: *Soil Sci. Soc. Amer. Proc.* **30,** 337–343.

Russell, J. D., Farmer, V. C., and Velde, B. (1970) Replacement of OH by OD in layer silicates, and identification of vibrations of these groups in infra-red spectra: *Mineral. Mag.* **37,** 869–879.

Telleria, M. I., Slade, P. G., and Radslovich, E. W. (1977) X-ray study of the interlayer region of a barium-vermiculite: *Clays & Clay Minerals* **25,** 119–125.

(Received 26 April 1979; accepted 24 October 1979)

Резюме—Описываются измерения дифракции нейтронов для преимущественно ориентированных агрегатных пластинчатых образцов детритового Na-монтмориллонита из Аптона, Вайоминг. Исследовались серии с содержанием воды в глине от 0 до 500 мг/г. Использованная длина волны нейтронов 2,39 Å и удаленные детекторы позволили собрать большинство «вне плоскостныз» компонентов дифракционных пиков интенсивностей.

Дифракционные картины интенсивностей от плоскостей 00ℓ глины, соответствующие отражающей геометрии, являются сильной функцией солержания воды в образце и показывают изменения основных промежутков от 9,0 до 19,0 Å. Отражения hk, полученные в результате трансмиссионных геометрических измерений показывают, однако, что *a*- и *b*-оси решетки постоянны в пределах погрешимости эксперимента 0,02 Å, связанной с определением содержания воды и что их интенсивности изменяются только на несколько процентов. В этой геометрии была замечена широкая, водо-подобная дифракционная картина, служащая фоном под обычной серией пиков интенсивностей hk. Эта фоновая водо-подобная картина изменяется пропорционально содержанию воды в образце.

Приемы восстановления данных включали рассмотрение удаления фона, многократного рассеивания, нормализации потока, и ослабления рассеивания из-за толщины образца. Анализ восстановленных данных показал, что вода в глине имеет структуру подобную жидкости с увеличенно плотностью примерно на 5% по сравнению с основной водой. Связь между несколькими межслойными молекулами воды и кремниевой суперструктурой определяется небольшим изменением интенсивности полос hk, но это изменение, по-видимому, заканчивается при содержании воды ниже 100 мг/г. Анализ Фурье базальной серии пиков от сухой глины показывает, что водород гидроксильных групп решетки находится в той же базальной плоскости как и их связанные кислородные атомы. [N. R.]

Resümee—Messungen der Neutronenbeugung an einer plattigen Probe aus einem besonders gut orietierten Aggregat von Deuterium-beladenen Na-Montmorillonit aus Upton, Wyoming, werden für eine Serie von Zwischenschichtwasser-Gehalten beschrieben, die von 0 bis 500 mg/g reichen. Eine Neutronenwellenlänge von 2,39 Å wurde zusammen mit vergrößerten Detektoren verwendet, um viel von der "out of plane"-Komponente der Beugungspeak-Intensitäten zu erhalten.

Die Intensität der Beugungsdiagramme der 00ℓ-Ebenen des Tons, die einer Spiegelgeometrie entsprechen, sind in starkem Maße vom Wassergehalt der Probe abhängig und zeigen eine Variation der Schichtabstände von 9,8 bis 19,0 Å. Die hk-Reflexe aus Transmissionsgeometriemessungen zeigen jedoch, daß die Gitterabstände auf der *a*- und *b*-Achse innerhalb der Meßgenauigkeit (0,02 Å) über den untersuchten Bereich der Wassergehalte konstant sind und ihre Intensitäten nur um einige Prozent schwanken. In dieser Geometrie wurde ein breites Beugungsdiagramm, das dem des Wassers ähnlich ist, als Untergrund unter den üblichen hk-Serien festgestellt. Dieses, dem des Wassers ähnliche Untergrunddiagramm variiert mit dem Wassergehalt der Probe.

Die Datenreduktion berücksichtigte Untergrundkorrektur, Mehrfachstreuung, Normalisierung des Neutronenflusses, und Schwächung der Streuung durch die Probendicke. Die Analyse der korrigierten Ergebnisse zeigte eine Flüssigkeit-ähnliche Struktur des Zwischenschichtwassers mit einem Dichtezuwachs von etwa 5% gegenüber "normalem" Wasser. Ein Zusammenhalt zwischen einigen Zwischenschichtwassermolekülen und dem Silikatgerüst ergibt sich aus der leichten Veränderung in den hk-Intensitäten. Diese Veränderung läßt sich jedoch nur bei Wassergehalten bis zu 100 mg/g nachweisen. Eine Fourier-Analyse der Basispeak-Serien des trockenen Tons zeigt, daß die Wasserstoffatome der Gitterhydroxylgruppen in der gleichen Basisebene liegen wie ihre assoziierten Sauerstoffatome. [U. W.]

Résumé—Des mesures de diffraction aux neutrons pour une plaque échantillon d'aggrégats orientée préferentiellement de montmorillonite-Na deutérée provenant d'Upton, Wyoming, sont décrites pour une série de contenus argile-eau s'étendant de 0 à 500 mg/g. Une longueur d'onde de neutron de 2,39 Å a été utilisée avec des détecteurs prolongés pour recueillir beaucoup du composant "hors de plan" des intensités du sommet de diffraction.

Les intensités du cliché de diffraction des plans 00ℓ de l'argile, correspondant à une géométrie de réflection, sont une réflection du contenu en eau de l'argile et montrent une variation d'espacement de base de 9,8 à 19,0 Å. Les réflections hk de mesures de géométrie de réflection montrent cependant que les axes *a* et *b* de l'édifice cristallin sont constants selon l'incertitude expérimentale (0,02 Å) pour l'étendue en contenu d'eau, et leurs intensités ne varient que de quelques pourcents. Dans cette géométrie, un large cliché de diffraction semblable à celui de l'eau a été remarqué comme arrière-plan sous les séries habituelles d'intensité de sommet hk. Ce cliché de fond semblable à celui de l'eau varie proportionellement avec le contenu en eau de l'échantillon.

Les démarches de réduction de données ont inclu la considération de l'enlèvement d'arrière-plan, de dispersion multiple, de normalisation de flux, et d'atténuation de dispersion à cause de l'épaisseur de l'échantillon. L'analyse des données réduites révèle que l'argile-eau a un ordre "semblable à un liquide," avec un accroissement de densité d'approximativement 5% par rapport à l'eau en masse. Une association entre quelques molécules d'eau intercouche et la superstructure de silice est indiquée par un léger changement dans les intensités de bandes hk, mais ce changement semble être completé à des teneurs en eau en dessous de 100 mg/g. L'analyse Fourier de la série des sommets de base de l'argile sec montre que les hydrogènes des groupes hydroxyles de l'édifice cristallin se trouvent dans le même plan de base que les atomes d'oxygène qui leur sont associés. [D. J.]